51st AIAA Aerospace Sciences Meeting including the New Horizons Forum and Aerospace Exposition
07 - 10 January 2013, Grapevine (Dallas/Ft. Worth Region), Texas

AIAA 2013-1064

SCAMP: Application of Nonlinear Progressive-wave Equation to Sonic Boom Transition Focus

Andrew A. Piacsek*
Central Washington University, Ellensburg, WA, 98926

Kenneth J. Plotkin†
Wyle, Arlington, VA, 22202

The Nonlinear Progressive-wave Equation (NPE) is one of three numerical models of focused sonic boom prediction being validated as part of the Superboom Caustic Analysis and Measurement Project (SCAMP). Formulated in the time domain, the NPE begins with a far-field acoustic signature and propagates it into the region with caustics, accounting for nonlinear steepening, refraction, dissipative processes, and narrow-angle diffraction. Proper initialization of the NPE requires scaling the sonic boom signature to a rippled wavefront that will generate the desired caustic curvature as it propagates. Details of the scaling and its limitations are described. Numerical results corresponding to SCAMP flight conditions are compared with measurements and results for low-boom conditions are presented.

Nomenclature

p	= acoustic pressure
ρ	= ambient density
c_0	= ambient sound speed
δ_{eff}	= effective dissipation coefficient for weak shocks in air
x	= propagation direction of computational domain
z	= transverse spatial coordinate of computational domain
β	= parameter of acoustic nonlinearity
$L_{\text{wf}}, R_{\text{wf}}$	= parameters describing ripple shape of initial sonic boom wavefront
P_{sh}	= peak amplitude of sonic boom signature
L_N	= length of sonic boom "N" wave
R_c	= radius of curvature of focusing caustic
μ	= nonlinear parameter in Tricomi scaling
δ	= diffraction layer thickness in Tricomi scaling
γ	= ratio of specific heats

I. Introduction

Because acceleration to supersonic speeds is a necessary maneuver for supersonic flight, a detailed understanding of the sonic boom focal zone is necessary for environmental assessment of commercial supersonic aircraft, as well as potential mitigation of the boom overpressures where focusing may occur. Accomplishing these goals is essential for the ultimate manufacture and operation of this kind of aircraft.

Early measurements of sonic booms from maneuvering flight[1-3] demonstrated significant amplification of boom amplitude in focal zones, as well as the potential for complex multi-signature patterns. The emphasis was on understanding the conditions that generated sonic boom focus, location of focus, and peak amplitude. Boom profiles were, in general, described qualitatively; in only one more recent experiment were peak pressures compared with quantitative models.[4]

* Assistant Professor, Dept. of Physics, 400 E. University Way, AIAA Senior member.
† Chief Scientist, EERC, 200 12th Street, Suite 900, AIAA Senior Member.

The recent development of computational models capable of describing sonic boom evolution during focusing, as well as the advent of shaped sonic booms, motivated the SCAMP project.[5-6] One of the models being investigated is the Nonlinear Progressive-wave Equation (NPE), developed by McDonald and Kuperman.[7] The NPE is a nonlinear time domain approach that resembles Burgers' equation with terms that account for off-axis propagation at moderate angles (diffraction) and refraction due to sound speed variations. The numerical implementation utilizes an effective shock capturing algorithm that avoids the use of artificial dissipation. Originally developed for underwater shock propagation, the NPE has been successfully adapted to sonic boom propagation in the atmosphere.[8] Recently, a "wide-angle" version of the NPE was developed by McDonald[9] that extends the angular range of validity; the new version, adapted for atmospheric propagation, is used for the SCAMP project.

II. Objectives

The objective of the SCAMP research program is to validate the physical formulation of three sonic boom focusing algorithms via flight test measurements, to recommend and apply code improvements if necessary and to apply these models to predict focus booms for low-boom aircraft designs.[10,11] The performance of the NPE algorithm is described in this paper.

As with the other focusing algorithms included in the SCAMP project, the NPE does not model sonic boom propagation from the source. The general approach uses a Computational Fluid Dynamics (CFD) program tailored to a particular aircraft to generate a near-field solution that is propagated with a ray-based algorithm (PCboom) as far as possible prior to the formation of caustics. The solution is then passed to each focus code for modeling propagation in the vicinity of caustics.

Specific objectives include developing a seamless procedure for incorporating the output of PCBoom as the starter field for NPE, determining the appropriate NPE grid dimensions and propagation time to the ground, making meaningful comparisons of NPE solutions with microphone signals from SCAMP flight tests, and identifying improvements to the NPE code.

III. Description of Methods

The NPE (Eq. 1) is formulated in the time domain,

$$\frac{\partial p}{\partial t} + c_0 \frac{\partial p}{\partial x} = -\frac{\partial}{\partial x}\left(c'p + \frac{\beta}{2}\frac{p^2}{\rho c_0} \right) - \frac{c_0}{2}\frac{\partial^2}{\partial z^2}\int_{\infty}^{x} p\,dx' + \delta_{\text{eff}}\frac{\partial^2 p}{\partial x^2} \tag{1}$$

The left hand side represents linear plane wave propagation; the terms on the right hand side represent, respectively, refraction and nonlinearity, diffraction, and dissipation. The x-axis represents the primary direction of wave propagation, while the wave front is nominally parallel to the z-axis. The wave is assumed to be uniform along the third Cartesian coordinate. In the present application, turbulence is neglected, so $c' = 0$ everywhere.

The solution of Eq. 1 utilizes a finite-difference scheme that marches forward in time. Each time step is split between the diffraction term (involving derivatives with respect to z) and the other terms (which involve derivatives with respect to x). The diffraction step uses an implicit Cranck-Nicholson solver, while the other step utilizes a Flux Corrected Transport (FCT) algorithm that handles the presence of shocks in the solution without the need for artificial dissipation. The computational domain moves with the ambient sound speed along the x direction, so that $t \to t - \frac{x}{c}$ and the time derivative in Eq. 1 corresponds to the time scale in this moving reference frame.

A two-dimensional pressure field is needed to initiate the NPE calculation. Far from the source, the sonic boom wavefront extends across the computatational domain with some region of undisturbed medium ahead of the bow shock and behind the tail shock. In the case of a focusing boom, the bow and tail shocks have moderate curvature that is concave in the direction of propagation, as shown in Fig. 1(a). Originally, it was expected that the initial field would be provided by the PCboom solution prior to, but near, the caustic. However, the geometry of the focusing sonic boom wave front and the associated caustic, made this approach to initializing the NPE solution unworkable.

Because the wave front is concave everywhere, it will be incoming at one or more boundaries of a rectangular domain, as seen in Fig. 1(a). Since information from an incoming wave cannot be modeled with a finite-difference scheme, interaction with the solution at such a boundary necessarily produces a diffracted or reflected wave that is not part of the physical solution. Figure 1(b) shows the solution, starting from the field plotted in Fig. 2a, after 12

seconds of propagation. Diffracted waves from the top and bottom boundaries have restricted the region of valid solution to a small section in the middle of the domain. After further propagation, the entire solution domain is corrupted by the diffracted waves.

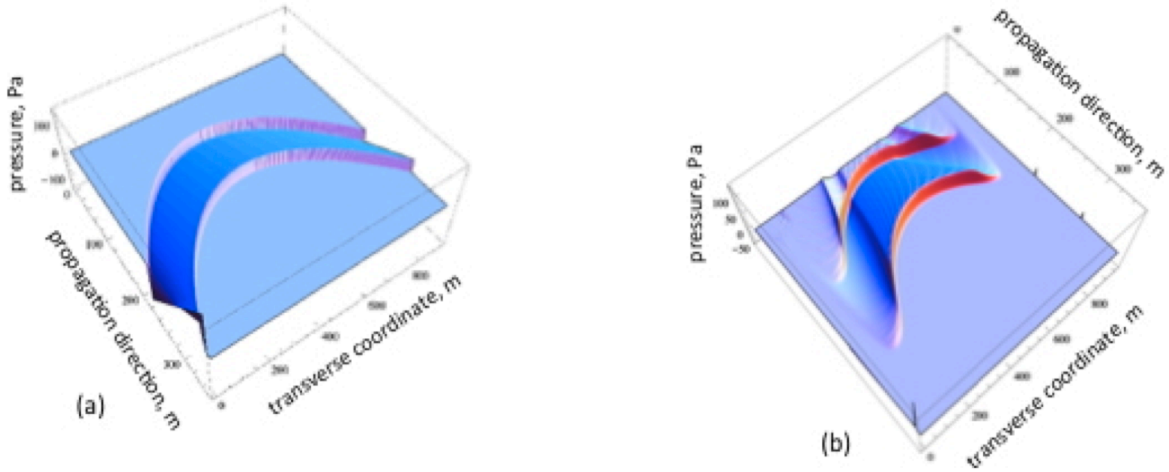

Figure 1. Plot of NPE solution as a 2-D acoustic pressure field, illustrating effects of wave truncation at the boundaries. (a) Initial NPE pressure field interpolated from PCboom. (b) NPE solution after 12 seconds of propagation.

In many circumstances, the domain size can be made large enough so that the unwanted diffracted wave does not corrupt the solution in the region of interest within the required propagation distance. In this case, however, the domain size is constrained by the presence of the caustic, as illustrated in Fig. 2. If the caustic has a sufficiently large radius of curvature, it is impossible to satisfy the competing constraints of ensuring that the caustic is not included within the initial NPE domain, while making the computational domain large enough to accommodate diffracted waves from the incoming shock front truncated at the boundaries.

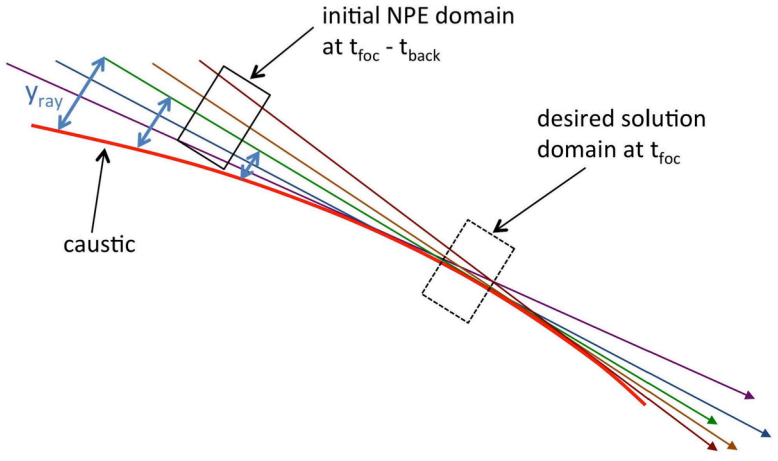

Figure 2. Location of NPE grid relative to the caustic. The initial computational domain, located at time t_{back} before focusing occurs, must lie outside of the caustic.

An alternative approach to initializing the NPE solution makes use of scaling laws for focusing shocks. The caustic is actually a surface shaped somewhat like a flaring trumpet horn, as illustrated in Fig. 3. The cusp of the

transition caustic is the location where the aircraft first goes supersonic. This caustic geometry can be approximated by propagating a nominally planar wavefront with a concave ripple that is specified by two parameters.[8] This wavefront, which is symmetric about the x-axis, is described by the following expression for the arrival time τ at $x = 0$ as a function of the transverse coordinate, z,

$$\tau_0(z) = \frac{L_{\text{wf}}}{c_0}\left[1 + \frac{L_{\text{wf}}}{2R_{\text{wf}}}\left(\frac{z}{L_{\text{wf}}}\right)^2\right]^{-1} \tag{2}$$

where c_0 is the ambient sound speed and the two wavefront shape parameters are the ripple depth L_{wf} and the minimum radius of curvature R_{wf}. In a sufficiently large computational domain, this wavefront will be nearly normal to the domain boundaries, eliminating the issue of diffraction emanating from a truncated incoming shock. Figure 3 shows an example of such a rippled wavefront, with R_{wf} = 1000m and L_{wf} = 100m, plotted at successive time intervals, together with the corresponding rays.

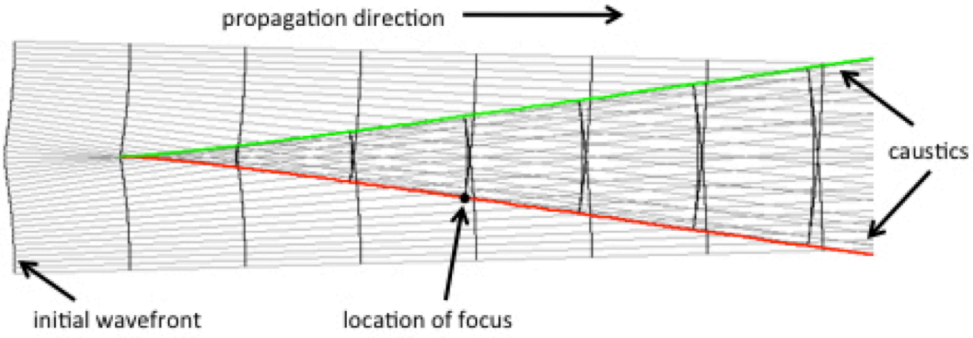

Figure 3. Rippled wavefront propagating to the right. Successive wavefronts at a constant time interval are shown with rays. The first focus, which is the location of the caustic cusp, occurs at the second wavefront. The shock originating in the upper portion of the first wavefront reflects off the bottom caustic.

The second wavefront in Fig. 3 is drawn to coincide with the point of first focus, which is the location of the caustic cusp. Beyond this point the wavefront exhibits folding, in which the shock is reflected at the caustic. A detailed view of this behavior, which is analagous to that of a sonic boom at focus, is illustrated in Figure 4.

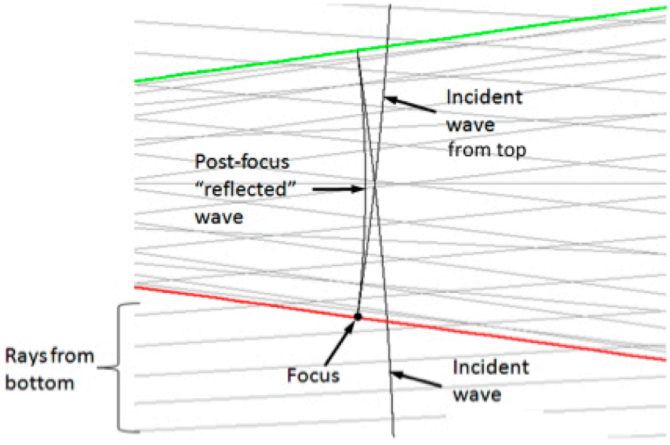

Figure 4. Detailed view of reflecting shock wave at the caustic.

The ripple parameters R_{wf} and L_{wf} are chosen to produce a local caustic curvature R_c that matches the conditions for a given SCAMP flight condition with appropriately scaled N-wave length and amplitude. The scaling is derived from the Nonlinear Tricomi Equation [12]

$$L_N = \left(\frac{2\delta^3}{R_c}\right)^{1/2} \quad \text{and} \quad P_{sh} = \mu \frac{\rho_0 c_0^2}{\gamma + 1}\left(\frac{2L_N}{R_c}\right)^{2/3} \tag{3}$$

Correspondence with SCAMP flight Maneuver C (-0.25 degree/second pushover while accelerating at 0.0035 Mach/second), for which the nonlinear parameter $\mu = 0.0737$ and diffraction layer thickness $\delta = 370$ m, was obtained using $L_N = 17.7$ m for the length of the N-wave and $P_{sh} = 10$ Pa for the shock amplitude, with $R_c = 313300$ m determined by ripple parameters R_{wf} and L_{wf} given above.

The NPE is initialized with a wavefront that is the bottom half of the leftmost wavefront depicted in Fig. 3. This rippled wavefront is normal to both the top and bottom boundaries, eliminating reflected waves. The top boundary is then the axis along which focusing occurs; the cusp is located on this axis, as illustrated in Figs. 3 and 4. As the solution propagates beyond the cusp, a caustic surface will grow into the NPE domain below the top boundary.

The spatial resolution of the NPE grid is $\Delta x = .05$ m in the direction of propagation and $\Delta z = .25$ m in the transverse direction; with $L_N = 17.7$ m, the N-wave is resolved with 354 grid points. The length of the NPE domain along the propagation axis is determined by the depth of the wavefront ripple L_{wf}, the N-wave length L_N, and the distance behind the initial N-wave needed to accommodate the lengthening N-wave and the reflected U-wave behind the caustic. The grid dimension along the transverse direction is large enough to ensure that the rippled wavefront is nearly normal to the bottom boundary (a quadratic curve that is exactly normal to the boundary is spliced to the rippled wavefront). The spatial resolution and domain size described above result in a computational grid with 4200x4200 elements.

It was determined that the time step Δt must be smaller than 1/20 Δx in order to avoid unstable ripple formation behind shocks. In the case reported here, $\Delta t = .002$ s. The solution was propagated to a distance of $4R_{wf} = 4000$m, where the shock at the caustic has the desired values of μ and δ. Approximately 12000 time steps were required.

IV. Results

The full NPE solution, $p(x,z)$ at a specific time step, is shown in Fig. 5(a), with important features labeled. Acoustic pressure is plotted along the vertical axis of this 3-D visualization. A subset of this solution, indicated by the dashed rectangle, is shown in Fig. 5(b) to provide detail. A comparison of these plots with the lower portion of Fig. 4 confirms that the overall wave front structure of the NPE solution corresponds to the ray tracing picture. The NPE solution also shows the transition from incident N-wave to reflected U-wave, as well as the evanescent region below the caustic.

Waveform slices from the 2-D NPE solution at 4000m are shown in Figure 5. Each slice is at a different distance from the top boundary, which is the axis of focus for the rippled wavefront. In Fig. 5(a), at a location 255m above the caustic, the N-wave that is incident upon the caustic is distinct from the U-wave that has reflected from the caustic. In Fig. 5(b), closer to the caustic, the N and U waves are overlapping. Figure 5(c) shows the maximum focus very close to the caustic. Below the caustic, only an evanescent wave exists, as shown in Figs. 5(d) and 5(e). The peak pressures are noted in the caption; amplitude scales are not identical for each profile.

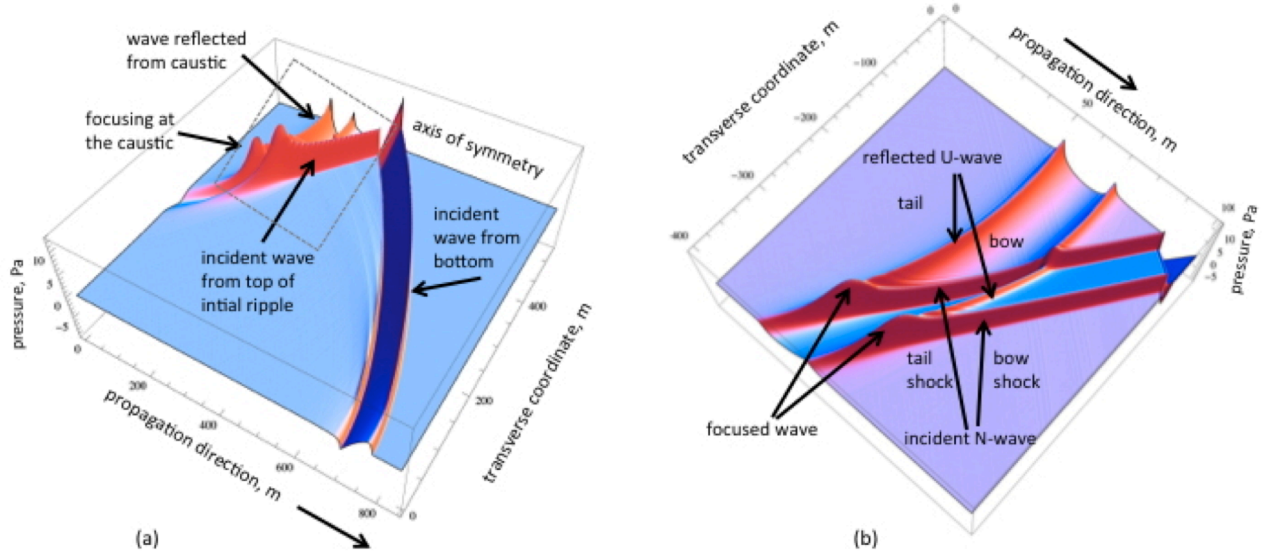

Figure 5. NPE solution at focus (propagation distance = 4000m), showing spatial distribution of acoustic pressure. (a) Full computational domain, showing incident and reflected waves. (b) Detailed view showing structure of incident N-wave and reflected U-wave in the vicinity of the caustic, as well as the evanescent wave field below the caustic.

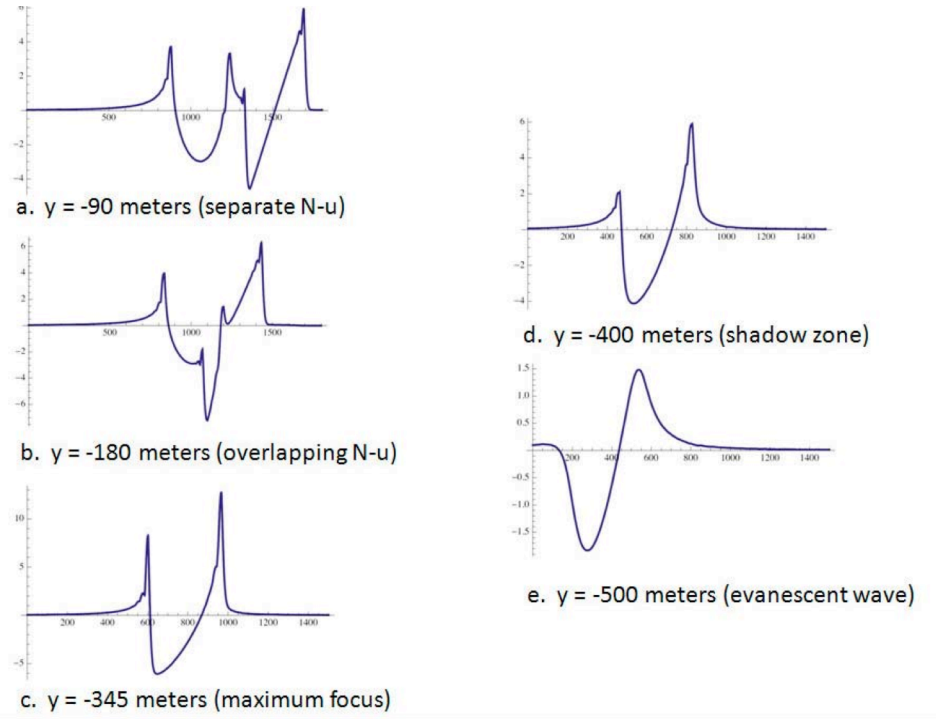

Figure 6. Wave profiles corresponding to slices of the NPE solution at several values of the transverse coordinate. Locations are in meters below the axis of symmetry. Each plot shows acoustic pressure vs. distance along the propagation axis.
Peak pressures are: (a) 5.97 Pa, (b) 6.30 Pa, (c) 12.79 Pa, (d) 5.90 Pa, (e) 1.48 Pa

In Fig. 7, the maximum focus NPE boom from Fig. 6(c) is compared to the maximum focus for five measured booms from SCAMP Maneuver C.[10] The calculated boom is rescaled and the coordinates have been transformed to p versus t.

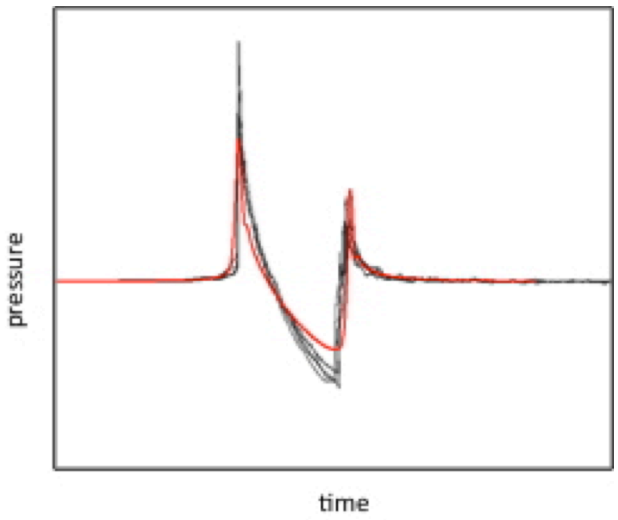

Figure 7. Comparison of NPE focused boom signature with five measured focus signatures from Maneuver C. Predicted peak pressure is 5.3 psf; measured peak pressures are 7.1, 6.6, 8.6, 8.8, and 6.3 psf.

The signature duration matches well and the shape is in general agreement. The predicted overpressure of 5.27 psf is somewhat lower than the measured peak pressures of 7.1, 6.6, 8.6, 8.8, and 6.3 psf. While the value of μ is close to the flight test value, the choice of δ placed the Tricomi boundary edge in a region that is converging differently from one closer to the caustic. An improvement to this method would be to propagate the signal a shorter distance, taking the solution at a location where R_c is smaller so that δ would be smaller. The signature length L_N used in the NPE calculation can also be shortened.

V. Focused Sonic Booms from Low Boom Vehicles

Transition focus booms were examined for three low boom configurations: a Gulfstream small (business jet) aircraft, a Boeing medium sized N+2 supersonic aircraft, and a NASA low-boom demonstrator. In each case, the NPE input signature is nominally the near field starting signature. That signature ages as it propagates, with aging in the atmosphere depending on the age parameter as computed by ray tracing in PCBoom. NPE propagation is two dimensional through a uniform atmosphere. Aging can be adjusted by either introducing a density gradient or adjusting the amplitude of the starting signature. For the current analysis, the initial amplitude was adjusted. An overall wave length of L_N =17.7 meters was necessary to avoid overlap between the leading and folded wave fronts; this was used for all cases. The initial amplitude was chosen such that, when the NPE signature at the edge of the focal zone was scaled back to chosen values of L_N and P_{sh}, the aging matched that of the delta-tangent signatures.

The Boeing N+2 low boom aircraft configuration was modeled assuming level flight at 40,000 ft accelerating at 0.5 knots/s. These flight conditions, similar to those reported in Ref. 6, produced the following Tricomi scaling parameters: R_c = 88.7 km, P_{sh} = 26 Pa, δ = 610 m, and L_N = 80 m. The NPE solution for this low boom configuration at the focus is shown in Fig. 8. Part (a) shows the signature at the edge of the focus, just clear of overlap from the wave originating from the lower half of the initial wavefront. Part (c) shows the maximum focus. Part (b) shows overlapping incident and reflected waves, while part (d) shows a wave in the shadow zone of the caustic. The sequence of waveforms is similar to that obtained from NTE solutions, although the coordinates of p versus x are reversed from the usual p versus t.

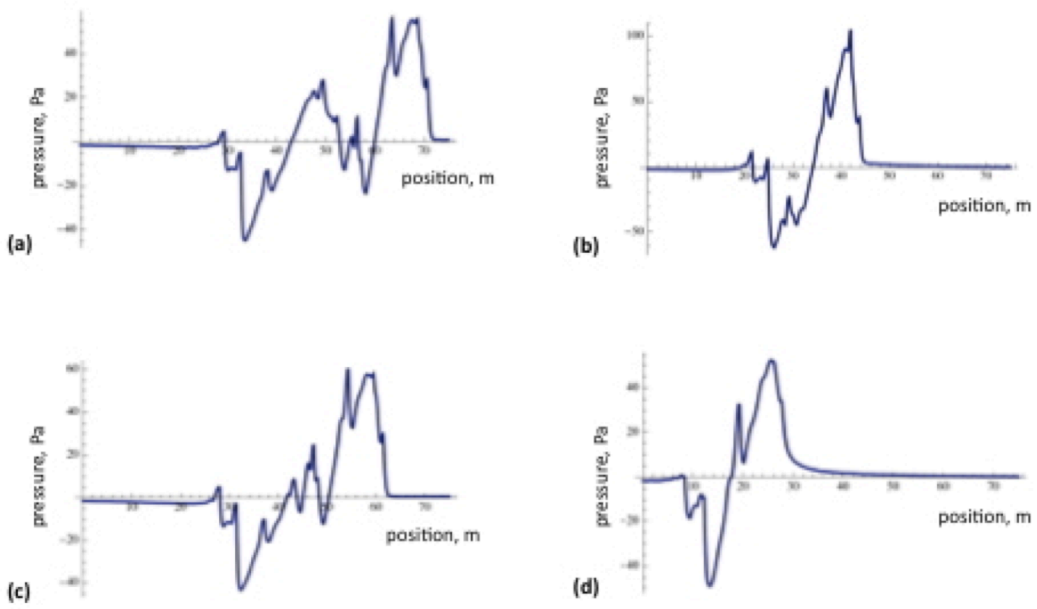

Figure 8. NPE solution at focus for Boeing N+2 low boom configuration. Profiles correspond to slices of the full pressure field at four distances from the focus axis: (a) Edge of focal zone at z = -85m. (b) Overlapping pre/post focus waves, z = -150 m. (c) Maximum focus, z = -245 m. (d) Evanescent zone, z = -400 m.

VI. Summary

The time-domain NPE model has been adapted to atmospheric propagation and applied to the problem of focused sonic booms. A significant challenge to implementing the NPE to booms created by maneuvering aircraft is determining a suitable starter field that incorporates the appropriate caustic geometry but does not contain the caustic. An approach that utilizes a rippled initial wavefront that is suitably scaled is described. Results for SCAMP Maneuver C show predicted boom signatures demonstrate the expected behavior of overlapping N and U waves on the illuminated side of the caustic and evanescent waves on the shadow side. The predicted waveform at maximum focus compares reasonably well to the measured waveform. Results for a focused Boeing low boom signature are also presented.

Acknowledgments

This project was sponsored by the National Aeronautics and Space Administration.

References

1. H. Hubbard, D. Maglieri, V. Huckel, and D. Hilton, "Ground measurements of sonic boom pressures for the altitude range of 10,000 to 75,000 feet," NASA TR R-198, July 1964.
2. D. Maglieri, D. Hilton, N. McLeod, "Experiments on the effects of atmospheric refraction and airplane accelerations on sonic boom ground pressure patterns," NASA TN D-3520, 1966.
3. J-C Wanner, J. Vallee, C. Vivier, and C. Thery, "Theoretical and experimental studies of the focus of sonic booms," J. Acoust. Soc. Am., **52**, 13-22 (1972).
4. M. Downing, N. Zamot, C. Moss, D. Morin, E. Wolski, S. Chung, K. Plotkin, and D. Maglieri, "Controlled focused sonic booms from maneuvering aircraft," J. Acoust. Soc. Am., **104**, 112-121 (1998).
5. Auger, T., Coulouvrat, F., "Numerical Simulation of Sonic Boom Focusing," AIAA Journal, **40**, 1726-1734 (2002).
6. Welge, H.R., et al., "N+3 Advanced Concept Studies for Supersonic Commercial Transport Aircraft Entering Service in the 2030-2035 Period," NASA Contractor Report NASA/CR-2011-217084, April 2011.
7. B. E. McDonald and W. Kuperman, "Time domain formulation for pulse propagation including nonlinear behaior at a caustic," J. Acoust. Soc. Am., **81**, pp. 1406-1417 (1987).

8. Piacsek, A., “Atmospheric turbulence conditions leading to focused and folded sonic boom wave fronts,” J. Acoust. Soc. Am. 111, 520-529 (2002).
9. B. E. McDonald, “High-angle formulation for the nonlinear progressive-wave equation model,” Wave Motion **31**, 165-171 (2002).
10. J. Page et al., “SCAMP: Superboom caustic analysis and measurement project overview,” 51st AIAA Aerospace Sciences Meeting, American Institute of Aeronautics and Astronautics, Reston, VA (submitted for publication).
11. Page, J. Plotkin, K., Hobbs, C. Sparrow, V. Salamone, J., Elmer, K., Ladd, J., Maglieri, D. and Piacsek, A., "Superboom Caustic Analysis and Measurement Program (SCAMP) Final Report," Wyle Report WR12-21, September 2012.
12. R. Marchiano, F. Coulouvrat, R. Grenon, "Numerical simulation of shock wave focusing at fold caustics, with application to sonic boom," J. Acoust. Soc. Am., **114**, 1758-1771 (2003).